



Real-time TWOS spectroscopy with sub-GHz resolution and high sensitivity

SRIKAMAL J. SOUNDARARAJAN AND LINGZE DUAN* 

Department of Physics & Astronomy, University of Alabama in Huntsville, Huntsville, AL 35899, USA

*lingze.duan@uah.edu

Abstract: A real-time spectroscopic technique called time-wavelength optical sampling (TWOS) is investigated. TWOS combines the concepts of time-stretch spectroscopy (TSS) and ultrafast optical sampling to address some of the challenges facing the conventional TSS, such as its overreliance on detector speed and the inherent tradeoff between spectral resolution and signal-to-noise ratio. Using optical sampling by laser cavity tuning (OSCAT), a spectral resolution of 710 MHz has been achieved in the 1.5 μm wavelength range. A 15-dB improvement in low-power tolerance and a frame rate as high as 2 kHz for real-time measurement are also demonstrated. This work sets the benchmark performance for TWOS spectroscopy and thereby lays out a path towards practical applications of this new technique.

© 2021 Optical Society of America under the terms of the [OSA Open Access Publishing Agreement](#)

1. Introduction

Real-time spectroscopy has garnered tremendous interest in recent years due to its potential to analyze the dynamics of chemical and biological reactions [1–5]. Conventional spectroscopic techniques such as grating-based spectrometers and Fourier transform-infrared spectroscopy (FTIR) generally suffer from long acquisition times and slow updating rates and thereby not suitable for real-time spectroscopy [1,6]. Meanwhile, novel techniques based on ultrafast lasers, in particular, time-stretch spectroscopy (TSS) and dual-comb spectroscopy, have shown great potential to achieve high spectral resolutions with fast frame rates [5–10].

Schematically, TSS is one of the simplest spectroscopic techniques. It exploits the concept of dispersive Fourier transform (or time lens) [11–13], mapping spectral profiles of ultrafast pulses into temporal distributions of optical power, which can be directly probed with high-speed photodetectors. Since each pulse carries the full spectrum of measurement, the frame rate of TSS can be as fast as the pulse repetition rate with the capability of making single-shot measurements [6]. However, the simplicity of this direct power-detection (DPD) scheme comes with some drawbacks. In TSS, high spectral resolution requires long pulse-stretching and fast photodetection. But both aspects face practical challenges. High-speed photodetectors are generally very expensive. Their response times are usually limited to about 10 ps and their bandwidths are typically below 100 GHz [14]. Moreover, such high-speed detectors are only available within selected wavelength ranges (e.g., visible, near-infrared). In other spectral regions, especially toward longer wavelengths, detector responses can be much slower. Therefore, relying on detector speed fundamentally restricts the applicability of TSS. Similar tradeoffs also occur in pulse stretching. A heavily stretched pulse has its energy spread across a large time span, effectively lowering the optical energy within each detector sampling window and hence reducing the signal-to-noise ratio (SNR). Although this problem can be mitigated by introducing distributed amplification in the dispersive fiber [5,15], considerably higher cost and complexity are also added to the system.

To address the deficiencies of the DPD scheme, we have previously proposed a new TSS scheme called time-wavelength optical sampling, or TWOS [16,17]. In TWOS, the stretched pulses are sampled *optically* by femtosecond laser pulses as opposed to electronically by the detector as in the DPD scheme. The photodetector, on the other hand, only measures the

cross-correlations between the stretched signal pulses and the femtosecond sampling pulses. This leads to two immediate benefits. First, the sampling window is now set by the duration of the sampling pulses rather than the detector speed, which decouples the detector response from the spectral resolution. In fact, “slow” detectors with bandwidths in the MHz range are generally sufficient for TWOS. Secondly, measuring the cross-correlations rather than the signal pulses themselves makes the SNR less susceptible to low signal power, because the sampling pulses also contribute to the detected optical power. This allows TWOS to work more reliably under low-light conditions. It also permits greater pulse-stretching and thereby better spectral resolutions. An additional advantage of TWOS is that the sampling windows are typically in the fs region, which is shorter than the DPD scheme by a factor of 10–100. This gives TWOS extra flexibility in time-stretching when a certain resolution is needed. Of course, these benefits come with tradeoffs. Since the sampling process requires periodic pulses within each scan or “frame”, TWOS is not able to make single-shot measurement. However, as will be shown later, the frame rate of TWOS can be as fast as multiple kHz, which is still sufficient for most applications that require real-time spectroscopy.

The key innovation that sets TWOS apart from the conventional DPD-based TSS is optical sampling. While there are a number of ways to realize optical sampling, the approach we have found particularly suitable for TWOS is optical sampling by laser cavity tuning, or OSCAT [18,19]. OSCAT combines an intracavity tuning of the pulse repetition rate with an extracavity, arm-length-imbalanced Mach-Zehnder interferometer (MZI) to achieve rapid scan of relative pulse delay [19]. It works especially well for TWOS because the long arm of the MZI, which typically ranges from hundreds of meters to several kilometers, can perform the dual-tasks of pulse stretching (for TSS) and pulse delay (for OSCAT). This results in a very simple and effective design of TWOS spectrometers [17]. To help readers understand the operating principle of OSCAT, a brief overview of the technique is given in Section 2.

While TWOS has been demonstrated in proof-of-principle studies, some important questions remain unanswered. For example, what is the limit of spectral resolution for TWOS and what are the limiting factors? How much improvement does TWOS have over DPD-based TSS in terms of power sensitivity? How fast can a TWOS spectrometer scan while making accurate measurement? In the work reported here, we seek to answer these questions by taking an in-depth study of the technique. In particular, our effort focuses on optimizing the performance of a TWOS spectrometer in the areas of spectral resolution (Section 3), power sensitivity (Section 4), and frame rate (Section 5). Conclusions are drawn in Section 6.

2. OSCAT overview

OSCAT belongs to a class of ultrafast optical sampling (UOS) techniques, which have gained strong momentum in recent years due to their broad range of applications in spectroscopy, remote sensing, biomedical imaging, metrology, etc. One of the first UOS schemes that attract widespread interest is asynchronous optical sampling (ASOPS) [20–24]. ASOPS uses two femtosecond lasers with a small repetition-rate detuning to create a rapid periodic scan of the relative pulse delay [23]. With two phase-locked frequency-comb lasers, ASOPS is able to downshift an optical spectral comb into the radio-frequency (RF) domain, resulting in an extremely high spectral resolution [25]. This feature leads to an emerging technology called dual-comb spectroscopy, which has seen tremendous growth over the last decade [9, 10, 26–28]. Dual-comb spectroscopy is especially suitable for real-time spectroscopy because of its fast frame rate, which can reach as high as MHz level [9,10,27].

However, the needs for *two* frequency-comb lasers and a phase-locking system add cost and complexity to a dual-comb scheme. Thus, there has been a constant effort to search for *single-comb* techniques that can offer similar performances. OSCAT is the first such scheme being widely exploited. OSCAT utilizes the simple fact that, when the output pulse train from

an ultrafast laser is injected into an armlength-imbalanced interferometer, changing the laser repetition rate would change the relative pulse delay between the two arms [18,19]. If the repetition rate is continuously modulated, a periodic scan of pulse delay is created, something exactly resembling ASOPS, except that only one laser is needed [19]. An important feature of OSCAT is its length-conversion capability, which can be mathematically described as [19]

$$\Delta l_d = (\Delta l_i / L_{c0}) \Delta L_c, \quad (1)$$

where L_{c0} and ΔL_c are the nominal laser cavity length and the cavity-length variation due to the intracavity modulation, respectively, and Δl_i and Δl_d are the armlength-imbalance of the interferometer and the relative pulse delay (in terms of length), respectively. Since the ratio $(\Delta l_i / L_{c0})$ is typically on the order of 10^4 , a μm -scale cavity-length modulation can lead to a cm -scale pulse-delay scan. This allows the use of high-speed piezoelectric (PZT) actuators for intracavity modulation, which have proved to be capable of operating at nearly 200 kHz [29]. The potential of achieving high frame rate has made OSCAT a legitimate single-comb alternative to some of the dual-comb schemes in the context of real-time spectroscopy.

Over the last few years, a number of applications of OSCAT have been explored [30–33]. In addition, several similar schemes based on laser repetition-rate tuning have also been developed [34–37], including optical sampling by repetition frequency modulation (OSREFM) [34] and optical sampling by electronic repetition-rate tuning (OSBERT) [36,37]. These prior efforts have demonstrated the effectiveness of OSCAT in achieving real-time measurement.

3. Spectral resolution

A conceptual layout of OSCAT-based TWOS spectrometers is shown in Fig. 1(a). An intracavity modulation to the fs laser creates a periodic change of the pulse repetition rate, which, by means of a highly armlength-imbalanced MZI, is turned into a periodic scan of the relative time delay between pulses going through the two arms of the MZI [19]. Meanwhile, group-velocity dispersion (GVD) causes the pulses traveling through the long arm of the MZI to be stretched, mapping their spectral profile into the time domain. The scan of the relative pulse delay between the two arms allows the *sampling* pulses from the short arm to “gate” the stretched *signal* pulses from the long arm in a fashion analogous to a “sliding window”. The resulted cross-correlation (interference) patterns are picked up by a photodetector and subsequently processed with an envelope-finding algorithm to recover the temporal profile of the signal pulses. With proper calibration, this temporal profile is mapped back to the spectral domain to obtain the signal

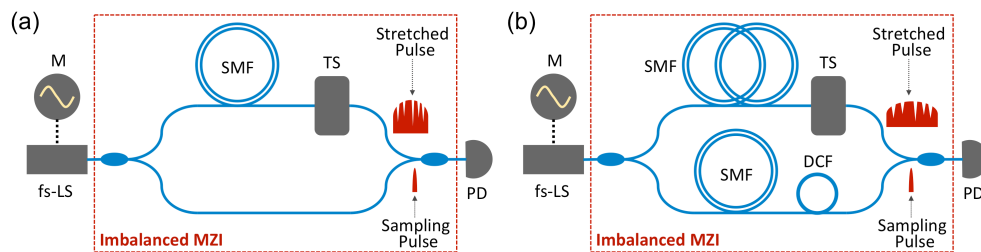


Fig. 1. (a) A block diagram of the TWOS spectrometer based on OSCAT. The time-stretched signal pulse (carrying the sample absorption lines) and the femtosecond sampling pulse are indicated. (b) Improved spectrometer design allows greater pulse stretching and hence better spectral resolutions. DCF, dispersion compensating fiber; fs-LS, femtosecond laser; M, modulator; PD, photodetector; SMF, single-mode fiber; and TS, test sample.

spectrum. The system makes one full scan of the spectrum within each period of the intracavity modulation. The modulation frequency determines the frame (updating) rate of the spectrometer.

For a TWOS spectrometer, in order to optimize its spectral resolution, the best scenario is to stretch the signal pulse as long as possible and compress the sampling pulse as short as possible. In fact, it has been shown that the theoretical minimum of the resolvable wavelength difference is given by [16]

$$\delta\lambda_{\text{TWOS}} = \frac{\Delta\tau_r}{|D|l_s}, \quad (2)$$

where $\Delta\tau_r$ is the sampling pulse width, D is the fiber GVD, and l_s is the length of the long arm. $\Delta\tau_r$ is dictated by the laser as well as pulse compression in the short arm. It is typically on the scale of 100 fs – 1 ps. l_s determines how long the pulses are stretched. For a particular laser, the maximum pulse duration after stretching is the inverse of its repetition rate (i.e., the time interval between adjacent pulses). Beyond this point, adjacent pulses begin to overlap, leading to possible measurement ambiguity. For example, our laser has a repetition rate of 250 MHz, which corresponds to a 4-ns maximum stretched pulse width. The corresponding maximum l_s is approximately 4 km.

However, in reality, the full benefit of the maximum pulse stretching is not necessarily attainable. Prior report has shown that, as the long arm becomes longer, the MZI imbalance also increases [17]. When the imbalance is above the coherence length of the laser, significant noise is generated in the cross-correlation signal, which hampers the recovery of the spectral profile and eventually restricts the length of the pulse-stretching fiber. For example, the best spectral resolution previously achieved with our TWOS spectrometer was 8 GHz (~ 60 pm), when the long arm was made of 400 m single-mode fiber (SMF) and the short arm was of a negligible length [17]. Further increasing the long arm (and hence pulse stretching) saw little improvement in spectral resolution due to the reduction of the SNR.

To overcome this limitation, two new approaches are taken in the current study. First, a 1.4-km fiber link is inserted into the short arm of the MZI. It consists of a 1.24-km SMF and a 142-m dispersion-compensating fiber (DCF). This combination creates a dispersion-balanced delay line, so that the sampling pulses (~400 fs in duration) can acquire a large time delay while preserving their pulse width at the end of the delay line. Meanwhile, with the short arm expanded to 1.4 km, the long arm can reach a total length of about 2 km before the imbalance of the MZI begins to cause degradation of the SNR. This allows the long arm to provide a much greater pulse stretching than the previous system. A conceptual layout of the modified system is shown in Fig. 1(b). Secondly, post-measurement denoising algorithms such as wavelet transform are used to digitally suppress the noise and recover the underlying spectral profiles. These measures enable the TWOS spectrometer to tolerate much greater noise caused by the MZI imbalance and hence allow the pulse-stretching fiber to be extended to beyond the limit set by the laser coherence length.

In fact, operation of the TWOS spectrometer has been demonstrated with a long arm comprising a 4-km pulse-stretching fiber. To facilitate the spectral-resolution measurement, a fiber Fabry-Perot (FP) interferometer (Micron Optics) is used as the test sample. The FP has a free-spectral range (FSR) of 100 GHz at a center wavelength of 1550 nm and a finesse of 1000, which results in a transmission linewidth of 100 MHz. The interrogation laser is a femtosecond fiber laser (Menlo Systems M-comb) operating at a center wavelength of 1540 nm with a repetition rate of 250 MHz. Figure 2(a) shows the periodic transmission peaks of the FP recovered by the TWOS spectrometer. The frequency scale is calibrated using the 100-GHz FSR of the FP. A zoom-in view of a single resonance peak is shown in Fig. 2(b). A full width at the half maximum (FWHM) of about 600 MHz is obtained in this particular instance. When averaged over multiple peaks, the mean value of the recovered transmission linewidth is found to be 710 MHz. This measured linewidth is apparently instrument-limited given the fact that the actual transmission

linewidth should be around 100 MHz. Thus, we conclude that the spectral resolution of the TWOS spectrometer is about 710 MHz, i.e., roughly 5.7 pm. It is worth pointing out that the best resolution reported using the conventional DPD scheme was 950 MHz, which was achieved by employing distributed Raman amplification [5].

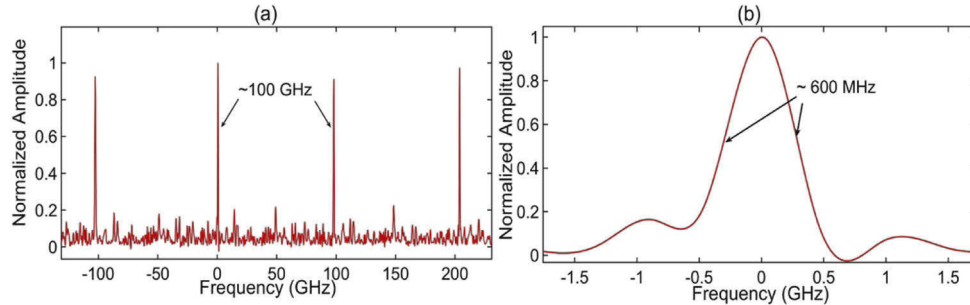


Fig. 2. (a) Periodic transmission peaks of the fiber FP interferometer recovered by the TWOS spectrometer. The center peak is arbitrarily chosen to highlight the 100-GHz FSR. (b) A zoom-in profile of a FP transmission peak shows a FWHM linewidth of about 600 MHz (the mean value over multiple peaks is about 710 MHz).

Meanwhile, there is still room for improvement with TWOS. The current sampling pulse width is estimated to be around 400 fs. A more careful pulse shaping/compression scheme can potentially bring $\Delta\tau_r$ down to about 100 fs, which would result in a three to four-fold improvement in spectral resolution. Pulse picking can also be applied to increase pulse-to-pulse spacing and thereby allow more pulse stretching.

4. Power sensitivity

Optical energy/power sensitivity is a critical parameter for spectrometers as it determines the ability of an instrument to operate under low light, which is a very common condition in measurements involving large background absorption or scattering [38,39]. As pointed out earlier, one of the advantages of TWOS in comparison with the conventional DPD-based TSS is its improved tolerance to low signal power. To quantitatively demonstrate this superiority, we have set up *both* schemes using the same components and compared their performances side by side.

Figure 3 shows the system configurations for (a) DPD-based TSS and (b) TWOS. In both cases, pulse stretching is accomplished with a 3.3-km SMF; a tunable fiber-optic attenuator (ATN) is inserted in the signal path to allow for adjustment of the optical power; and a 5-GHz InGaAs photodetector (Thorlabs DET08CF8C) is used as the signal receiver. The characteristic double-peak spectrum of the laser, as shown in the Fig. 4(b) inset, serves as the beacon in the measurements. In each case, the optical power incident on the detector *from the signal path* is gradually lowered by adjusting the ATN, until the receiver is no longer able to faithfully recover the double-peak feature of the laser spectrum.

The results are summarized in Fig. 4. Figure 4(a) shows the temporal profiles of the stretched pulses recovered by the DPD method under three average power levels: 145 μW , 75 μW and 45 μW . At 145 μW and 75 μW , the pulse shape resembles the laser spectrum with the characteristic double-peak feature, although the resolution is relatively low due to the slow response of the oscilloscope used in these measurements (Tektronix MDO4104, 1 GHz). At 45 μW , however, the stretched pulse no longer carries a clear double-peak feature, indicating a compromise of the recovery fidelity because of the degradation of SNR. On the other hand, Fig. 4(b) shows the laser spectrum measured by TWOS under three different power levels (the power through the long arm

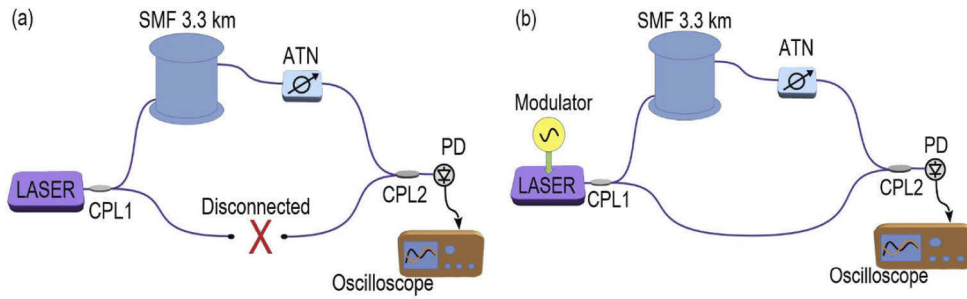


Fig. 3. (a) The experimental system layout for DPD-based TSS (the short arm is disconnected). (b) System layout for TWOS. ATN, variable optical attenuator; CPL, fiber coupler; PD, photodetector; and SMF, single-mode fiber.

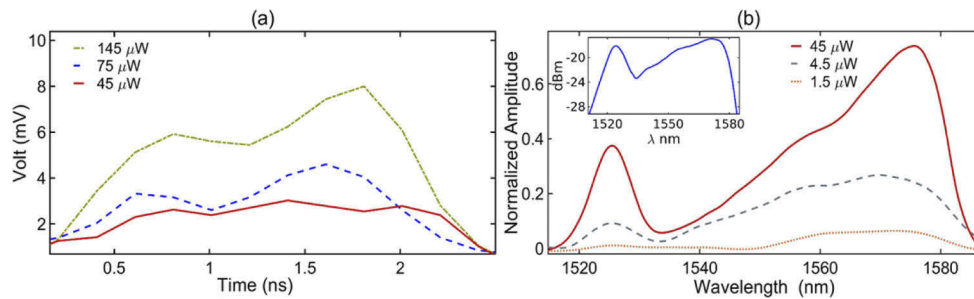


Fig. 4. (a) Time-domain profiles of the stretched pulses measured by the DPD method at three average power levels. The double-peak shape of the laser spectrum is recognizable at $145 \mu\text{W}$ and $75 \mu\text{W}$ but becomes unclear at $45 \mu\text{W}$. (b) The laser spectra recovered by TWOS at three average power levels, in comparison with the actual laser spectrum (shown here as inset). Good recovery fidelity is achieved at $45 \mu\text{W}$ and $4.5 \mu\text{W}$. The double-peak feature becomes obscure at $1.5 \mu\text{W}$, representing a roughly 15 dB improvement from the DPD method.

only): $45 \mu\text{W}$, $4.5 \mu\text{W}$ and $1.5 \mu\text{W}$. It is clear that TWOS is able to faithfully recover the laser spectrum at power levels as low as $4.5 \mu\text{W}$ and its measurement reliability only begins to degrade at $1.5 \mu\text{W}$. This is an approximately 15-dB improvement from the DPD-based TSS.

The reason for this improvement is very easy to understand. In the DPD scheme, the detection of the pulse waveforms completely relies on the optical power of the stretched pulses (through the upper link in Fig. 3(a)). If the specimen has a high optical attenuation, which is simulated here by the ATN, the optical power reaching the photodetector can be so low that system noises, such as detector noise or instrument noise, begin to limit measurement accuracy. For example, in the current case, the electronic noise in the oscilloscope is believed to be the dominant noise source. Given an optical power of $45 \mu\text{W}$ on the photodetector, a detector responsivity of 0.9 A/W , and a termination impedance of 50Ω , the average voltage signal generated on the oscilloscope is about 2 mV. This signal level is comparable to the 0.2-mW random noise specified for the oscilloscope, which has begun to hinder the recovery of the waveform as shown by the bottom (solid) trace in Fig. 4(a).

Meanwhile, the situation is quite different in TWOS. The addition of the sampling pulses (through the bottom arm in Fig. 3(b)) effectively introduces a “local oscillator” in an optical mixing scheme. The amplitude of the cross-correlation signal generated by the photodetector is proportional to $\sqrt{I_s I_r}$, where I_s and I_r are the average power of the signal arm and the sampling arm, respectively. In our experiment, I_r is approximately 1 mW. If $I_s = 45 \mu\text{W}$, the voltage signal

on the oscilloscope is about 10 mV, which is considerably higher than the DPD-generated voltage at the same power level. This explains why TWOS is able to tolerate much lower optical signal powers. It is also easy to confirm that, when $I_s = 1.5 \mu\text{W}$, the voltage signal on the oscilloscope drops below 2 mV. This is where the accuracy of TWOS begins to degrade, as shown by the dotted trace in Fig. 4(b).

Note that the improvement in power sensitivity over the DPD scheme can be even greater for TWOS with a higher sampling power I_r , and, in principle, such an improvement is independent of the detector or the measurement instrument (e.g., oscilloscope) being used because it occurs in the optical domain. A quick analysis shows that, under the same experimental conditions, TWOS can enjoy a power advantage of I_r/I_s in comparison with DPD-based TSS. This assessment is consistent with our experimental observation.

5. Real-time spectroscopy

To evaluate the full potential of the TWOS spectrometer in real-time spectroscopy, we have measured the absorption spectrum of hydrogen cyanide (HCN) at fast frame rates. The HCN sample is a 5-cm long glass gas cell at a pressure of 330 Torr. It is placed in between a multi-pass mirror pair, and the entire unit is inserted in the TWOS spectrometer as shown in Fig. 1(a). For this demonstration, the short arm of the MZI has a negligible length, while the long arm consists of a 1.4-km dispersion-compensated delay line as well as an extra 40-m SMF for pulse stretching. This particular configuration has been chosen because it enables us to observe the full absorption band of HCN from 1530 nm to 1560 nm within one scan. The scan of the pulse delay is accomplished by electrically modulating a PZT actuator (20 kHz bandwidth) attached to an intracavity mirror in the femtosecond laser. When driven at its full range, the PZT can cause a change of the pulse repetition rate by 3.55 kHz (out of a nominal rep rate of 250 MHz). Practically, however, the modulation depth is often less than the full range to avoid damage to the PZT. Especially at high frequencies (e.g., above 1 kHz), the amplitude of the modulation is further reduced to prevent potential damage of the mirror assembly.

Figure 5(a) shows a time-domain cross-correlation trace measured at a frame rate of 400 Hz. The outer profile (blue) is taken without the HCN sample. It serves as a reference trace to help remove the background laser spectrum. The inner profile (red) is taken with the HCN sample. Its corrugated envelope indicates spectral features caused by atomic absorption. By subtracting the laser background out of the time-domain signal and using a proper calibration procedure, a full spectrogram of the HCN absorption band is recovered, as shown in Fig. 5(b). The spectrogram spans across a wavelength range of more than 30 nm and clearly reveals the *R* and *P* branches of HCN in the near-infrared region. The double-dip feature bears a high similarity to the standard HITRAN-archived spectrum as shown in the inset.

More spectral details can be revealed by “zooming” the spectrometer into a selected region of the full absorption spectrum. This is done by adjusting the intracavity-modulation amplitude and offset. Reducing the modulation amplitude also allows us to further increase the modulation frequency, leading to much higher scanning frame rates. Figure 6(a) shows the full *R* branch of HCN measured at a 1-kHz frame rate. The absorption peaks are compared with the HITRAN data, which are indicated here by the dotted grid, and show very good agreements. An even higher frame rate of 2 kHz has also been achieved by scanning a portion of the *R* branch, as shown in Fig. 6(b). In this case, each scan takes only 500 μs and covers a spectral range of over 5 nm, which demonstrates the potential of TWOS as a practical technique for real-time spectroscopy. Once again, comparisons with the archived HITRAN data indicate a high degree of measurement accuracy.

Note that all the spectral traces presented in Fig. 5 and Fig. 6 are single-scan traces, i.e., no multi-trace averaging is needed. As to measurement errors, there are three major sources of error in the current setup. First, uncertainty in the calibration process may cause calibration

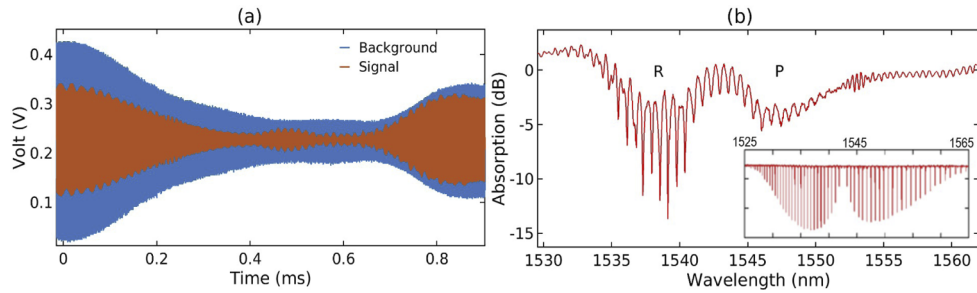


Fig. 5. (a) Time-domain traces measured by the TWOS spectrometer with (*signal*) and without (*background*) the HCN sample cell. The corrugated envelope of the *signal* trace indicates the atomic absorption features of HCN. (b) A full absorption spectrum of HCN in near infrared is recovered by the TWOS spectrometer at a frame rate of 400 Hz, showing clearly both the *R* and the *P* branches and in good agreement with the standard HCN absorption spectrum (inset).

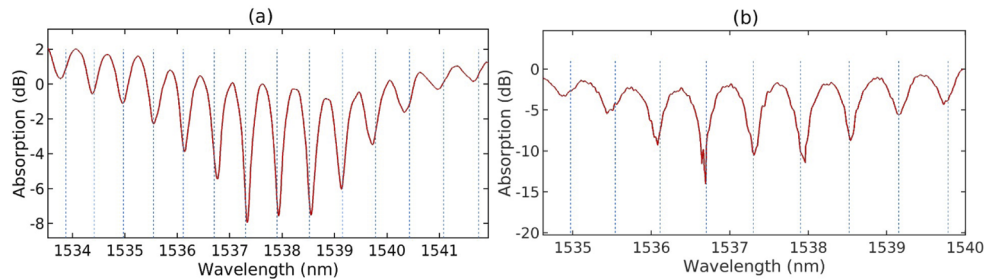


Fig. 6. Zoomed-in views of the HCN *R* branch measured by the TWOS spectrometer at frame rates of (a) 1 kHz and (b) 2 kHz, respectively. Dotted grids indicate the standard HITRAN absorption lines for HCN.

error. The measurement results presented here are calibrated using the double-peak feature of the laser spectrum, which is relatively broad. It proves to be effective in the current context, but narrow-linewidth atomic absorption features will have to be used for improved accuracy. Secondly, fluctuations of the laser cavity length cause slow drift of the pulse repetition rate, which ultimately affects the accuracy of the recovered spectrum. This effect can be mitigated by applying thermal and acoustic isolation to the laser cavity to improve its stability. Finally, nonlinear PZT response results in a nonconstant speed of pulse scan, which can skew the time-to-wavelength mapping. The speed profile, however, can be measured with the help of a periodic spectral feature such as the transmission lines of a fiber FP interferometer. Thus, in principle, PZT nonlinearity can be calibrated off.

The main limiting factors of the frame rate in our TWOS spectrometer are the bandwidth of the PZT actuator and the mechanical stability of the intracavity mirror. These technical challenges, however, can in principle be mitigated by enlisting PZT actuators with wider bandwidths and employing mirror assemblies specifically engineered for such purposes. For references, PZT-actuated intracavity mirrors with a bandwidth of 180 kHz have been experimentally demonstrated [29].

6. Conclusion

In conclusion, a new time-stretch technique called TWOS has been investigated. TWOS incorporates the concept of optical sampling into the TSS scheme and thereby addresses some

of the challenges facing the conventional DPD-based TSS such as its overreliance on detector speed and the inherent tradeoff between spectral resolution and SNR. We have performed a comprehensive study on TWOS spectroscopy with a special focus on maximizing its potential in spectral resolution, power sensitivity and real-time measurement. Spectral resolutions as high as 710 MHz has been achieved in the 1.5 μm wavelength range. A 15-dB improvement in low-power tolerance in comparison with DPD-based TSS has been demonstrated. Finally, real-time spectroscopic measurements on an HCN gas sample have been accomplished with frame rates as high as 2 kHz and good accuracy. This work sets the benchmark performance for TWOS spectroscopy and thereby lays out a path towards practical applications of this new technique. It should be stressed here that the concept of TWOS is generic and its application is not restricted to spectroscopy. Many other fields can find use of this idea, including optical ranging, imaging, metrology and sensing.

Funding. National Science Foundation (ECCS-1254902, ECCS-1606836); National Aeronautics and Space Administration (80NSSC19M0033).

Disclosures. The authors declare no conflicts of interest.

Data availability. Data underlying the results presented in this paper are not publicly available at this time but may be obtained from the authors upon reasonable request.

References

1. N. V. Tkachenko, *Optical spectroscopy: methods and instrumentations* (Elsevier, 2006).
2. K. Sokolov, M. Follen, and R. Richards-Kortum, "Optical spectroscopy for detection of neoplasia," *Curr. Opin. Chem. Biol.* **6**(5), 651–658 (2002).
3. K. D Skeldon, C. Patterson, C. A. Wyse, G. M. Gibson, M. J. Padgett, C. Longbottom, and L. C. McMillan, "The potential offered by real-time, high-sensitivity monitoring of ethane in breath and some pilot studies using optical spectroscopy," *J. Opt. A: Pure Appl. Opt.* **7**(6), S376–S384 (2005).
4. J. Hult, R. S. Watt, and C. F. Kaminski, "High bandwidth absorption spectroscopy with a dispersed supercontinuum source," *Opt. Express* **15**(18), 11385–11395 (2007).
5. J. Chou, D. R. Solli, and B. Jalali, "Real-time spectroscopy with sub-gigahertz resolution using amplified dispersive Fourier transformation," *Appl. Phys. Lett.* **92**(11), 111102 (2008).
6. K. Goda and B. Jalali, "Dispersive Fourier transformation for fast continuous single-shot measurement," *Nature Photon* **7**(2), 102–112 (2013).
7. R. R. Thomson, "Time-stretch spectroscopy STEAMs ahead," *Laser Focus World* **53**, 41 (2017).
8. A. Mahjoubfar, D. V. Churkin, S. Barland, N. Broderick, S. K. Turitsyn, and B. Jalali, "Time stretch and its applications," *Nature Photon* **11**(6), 341–351 (2017).
9. T. Ideguchi, A. Poisson, G. Guelachvili, N. Picqué, and T. W. Hänsch, "Adaptive real-time dual-comb spectroscopy," *Nat Commun* **5**(1), 3375 (2014).
10. I. Coddington, N. Newbury, and W. Swann, "Dual-comb spectroscopy," *Optica* **3**(4), 414–426 (2016).
11. T. Jansson, "Real-time Fourier transformation in dispersive optical fibers," *Opt. Lett.* **8**(4), 232–234 (1983).
12. B. H. Kolner and M. Nazarathy, "Temporal imaging with a time lens," *Opt. Lett.* **14**(12), 630–632 (1989).
13. V. Torres-Company, D. E. Leaird, and A. M. Weiner, "Dispersion requirements in coherent frequency-to-time mapping," *Opt. Express* **19**(24), 24718–24729 (2011).
14. H.-G. Bach, A. Beling, G. G. Mekonnen, R. Kunkel, D. Schmidt, W. Ebert, A. Seeger, M. Stollberg, and W. Schlaak, "InP-based waveguide-integrated photodetector with 100-GHz bandwidth," *IEEE J. Select. Topics Quantum Electron.* **10**(4), 668–672 (2004).
15. D. R. Solli, J. Chou, and B. Jalali, "Amplified wavelength–time transformation for real-time spectroscopy," *Nature Photon* **2**(1), 48–51 (2008).
16. S. J. Soundararajan, L. Yang, S. Zhang, H. Jani, and L. Duan, "Time-wavelength optical sampling spectroscopy based on dynamic laser cavity tuning," *J. Opt. Soc. Am. B* **35**(5), 1186–1191 (2018).
17. S. J. Soundararajan and L. Duan, "Time-stretch spectroscopy based on laser cavity tuning with a dual-function delay line," *IEEE Photonics Technol. Lett.* **27**, 1761–1764 (2019).
18. T. Hochrein, R. Wilk, M. Mei, R. Holzwarth, N. Krumbholz, and M. Koch, "Optical sampling by laser cavity tuning," *Opt. Express* **18**(2), 1613–1617 (2010).
19. L. Yang, J. Nie, and L. Duan, "Dynamic optical sampling by cavity tuning and its application in lidar," *Opt. Express* **21**(3), 3850–3860 (2013).
20. A. Bartels, R. Cerna, C. Kistner, A. Thoma, F. Hudert, C. Janke, and T. Dekorsy, "Ultrafast time-domain spectroscopy based on high-speed asynchronous optical sampling," *Rev. Sci. Instrum.* **78**(3), 035107 (2007).
21. C. Janke, M. Först, M. Nagel, and H. Kurz, "Asynchronous optical sampling for high-speed characterization of integrated resonant terahertz sensors," *Opt. Lett.* **30**(11), 1405–1407 (2005).

22. J. T. Good, D. B. Holland, I. A. Finneran, P. B. Carroll, M. J. Kelley, and G. A. Blake, "A decade-spanning high-resolution asynchronous optical sampling terahertz time-domain and frequency comb spectrometer," *Rev. Sci. Instrum.* **86**(10), 103107 (2015).
23. O. Kliebisch, D. C. Heinecke, and T. Dekorsy, "Ultrafast time-domain spectroscopy system using 10 GHz asynchronous optical sampling with 100 kHz scan rate," *Opt. Express* **24**(26), 29930–29940 (2016).
24. H. Shi, Y. Song, J. Yu, R. Li, M. Hu, and C. Wang, "Quantum-limited timing jitter characterization of mode-locked lasers by asynchronous optical sampling," *Opt. Express* **25**(1), 10–19 (2017).
25. I. Coddington, W. C. Swann, and N. R. Newbury, "Coherent multiheterodyne spectroscopy using stabilized optical frequency combs," *Phys. Rev. Lett.* **100**(1), 013902 (2008).
26. B. Bernhardt, A. Ozawa, P. Jacquet, M. Jacquy, Y. Kobayashi, T. Udem, R. Holzwarth, G. Guelachvili, T. W. Hänsch, and N. Picqué, "Cavity-enhanced dual-comb spectroscopy," *Nature Photon* **4**(1), 55–57 (2010).
27. F. Zhu, T. Mohamed, J. Strohaber, A. A. Kolomenskii, T. Udem, and H. A. Schuessler, "Real-time dual frequency comb spectroscopy in the near infrared," *Appl. Phys. Lett.* **102**(12), 121116 (2013).
28. M. A. Abbas, Q. Pan, J. Mandon, S. M. Cristescu, F. J. M. Harren, and A. Khodabakhsh, "Time-resolved mid-infrared dual-comb spectroscopy," *Sci. Rep.* **9**(1), 17247 (2019).
29. T. C. Briles, D. C. Yost, A. Cingöz, J. Ye, and T. R. Schibli, "Simple piezoelectric-actuated mirror with 180 kHz servo bandwidth," *Opt. Express* **18**(10), 9739–9746 (2010).
30. S. Boudreau and J. Genest, "Range-resolved vibrometry using a frequency comb in the OSCAT configuration," *Opt. Express* **22**(7), 8101–8113 (2014).
31. L. Yang and L. Duan, "Depth-resolved imaging based on optical sampling by cavity tuning," *IEEE Photonics Technol. Lett.* **27**(16), 1761–1764 (2015).
32. K. Lee, J. Lee, Y.-S. Jang, S. Han, H. Jang, Y.-J. Kim, and S.-W. Kim, "Fourier-transform spectroscopy using an Er-doped fiber femtosecond laser by sweeping the pulse repetition rate," *Sci. Rep.* **5**(1), 15726 (2015).
33. H. Wu, F. Zhang, T. Liu, P. Balling, J. Li, and X. Qu, "Long distance measurement using optical sampling by cavity tuning," *Opt. Lett.* **41**(10), 2366–2369 (2016).
34. T. Furuya, E. S. Estacio, K. Horita, C. T. Que, K. Yamamoto, F. Miyamaru, S. Nishizawa, and M. Tani, "Fast-scan terahertz time domain spectrometer based on laser repetition frequency modulation," *Jpn. J. Appl. Phys.* **52**(2R), 022401 (2013).
35. M. I. Kayes and M. Rochette, "Fourier transform spectroscopy by repetition rate sweeping of a single electro-optic frequency comb," *Opt. Lett.* **43**(5), 967–970 (2018).
36. D. Bajek, "High-Speed Optical Sampling Techniques Enabled by Ultrafast Semiconductor Lasers," in Ch. 4. 2016, University of Dundee.
37. D. Bajek and M. A. Cataluna, "Fast optical sampling by electronic repetition-rate tuning using a single mode-locked laser diode," *Opt. Express* **29**(5), 6890–6902 (2021).
38. W. Slavin, G. R. Carnrick, and S. R. Koertyohann, "Background correction in atomic absorption spectroscopy (AAS)," *Crit. Rev. Anal. Chem.* **19**(2), 95–134 (1988).
39. Y. Mendelson, A. C. Clermont, R. A. Peura, and B. C. Lin, "Blood glucose measurement by multiple attenuated total reflection and infrared absorption spectroscopy," *IEEE. Trans. Biomed. Eng.* **37**(5), 458–465 (1990).